Nonadiabatic transitions in non-Hermitian $\mathcal{PT}$-symmetric two-level systems

Jian-Song Pan[1,2,*] and Fan Wu[3,†]

[1]*College of Physics, Sichuan University, Chengdu 610065, China*

[2]*Key Laboratory of High Energy Density Physics and Technology of Ministry of Education, Sichuan University, Chengdu 610065, China*

[3]*Fujian Key Laboratory of Quantum Information and Quantum Optics, College of Physics and Information Engineering, Fuzhou University, Fuzhou, Fujian 350108, China*

(Received 1 February 2023; revised 13 November 2023; accepted 13 February 2024; published 28 February 2024)

We systematically characterize the dynamical evolution of time-parity ($\mathcal{PT}$)-symmetric two-level systems with spin-dependent dissipations. If the control parameters of the gap are linearly tuned with time, the dynamical evolution can be characterized with parabolic cylinder equations which can be analytically solved. We find that the asymptotic behaviors of particle probability on the two levels show initial-state-independent redistribution in the slow-tuning-speed limit as long as the system is nonadiabatically driven across exceptional points. Equal distributions appear when the nondissipative Hamiltonian shows gap closing. As long as the nondissipative Hamiltonian displays level anticrossing, the final distribution becomes unbalanced. The ratios between the occupation probabilities are given analytically. These results are confirmed with numerical simulations. The predicted equal-distribution phenomenon may be used to identify the closing of the energy gap from anticrossing between two energy bands.

DOI: 10.1103/PhysRevA.109.022245

I. INTRODUCTION

The past few decades have witnessed the rapid growth of research interest in non-Hermitian systems with parity-time ($\mathcal{PT}$) symmetry [1–25]. These systems possess real (conjugate complex) spectra in the $\mathcal{PT}$-symmetric (breaking) phases [1–3]. The spontaneous breaking of $\mathcal{PT}$ symmetry by spin-dependent dissipation (or gain and loss in optics) leads to the emergence of an exceptional point (EP) with the coalescence of eigenstates, which has been experimentally checked on different platforms [4–17]. The singular character of EPs not only is useful for sensing [26–28] but also has a profound impact on the dynamics of the system, exemplified by the phenomenon of chiral state transfer in the dynamical evolution surrounding EPs [19,22–25,29].

Furthermore, when a $\mathcal{PT}$-symmetric two-level system is driven directly through EPs, the transition probability shows anomalous asymptotic behaviors [30]. In the adiabatic limit, an equal redistribution between the states coalescing at the exceptional points is observed. Equal redistribution was numerically shown to be independent of the initial states. However, only a typical $\mathcal{PT}$-symmetric model, $H = \eta\sigma_z + i\gamma\sigma_x$, has been taken into account. In fact, a generic $\mathcal{PT}$-symmetric model should take the form of $H = \eta\sigma_z + \delta_0\sigma_0 + \delta_y\sigma_y + i\gamma\sigma_x$ [31]. The natural question then is whether these phenomena are preserved for the generic $\mathcal{PT}$-symmetric two-level model. Other questions include whether the loss of initial information can be analytically proven and how the additional real σ_y term influences the asymptotic redistribution. To answer these questions, a systematic study of the nonadiabatic transition of the generic $\mathcal{PT}$-symmetric model is required.

In this work, we systematically characterize the nonadiabatic time evolution of the generic $\mathcal{PT}$-symmetric non-Hermitian two-level model with spin-dependent dissipations. The nondissipative Hamiltonian shows gap closing or anticrossing when it possesses $\mathcal{PT}$ symmetry and shows level anticrossing when the $\mathcal{PT}$ symmetry is absent. A section of imaginary spectra ending with EPs ($\mathcal{PT}$-symmetry-breaking bubble) emerges, provided that the $\mathcal{PT}$ symmetry is broken and restored by tuning the gap-control parameter. When the energy-gap-control parameter is tuned to cross the EPs, the particle probabilities of nonadiabatic evolution are shown to be redistributed on the two levels in the slow-tuning-speed limit. The probability ratio between the two levels is a constant determined by the Hamiltonian parameters which is independent of the initial states.

We find that the asymptotic behavior of equal distribution exists only when the nondissipative Hamiltonian shows the closure of the gap, that is, the case studied in Ref. [30]. The redistribution becomes unbalanced if the nondissipative Hamiltonian displays level anticrossing, i.e., the current case with the generic $\mathcal{PT}$-symmetric model. These analytical results are confirmed by numerical simulations. For comparison, cases without $\mathcal{PT}$ symmetries in which the initial-state-independent asymptotic behavior disappears are also addressed. It is worth emphasizing that the redistribution asymptotic behavior is in sharp contrast to the Landau-Zener-Stückelberg interference in a common Hermitian system, where the final state sensitively depends on the initial condition.

Many interesting physical processes, such as first-order quantum phase transitions, are signaled by closing the energy

*panjsong@scu.edu.cn

†T21060@fzu.edu.cn

TABLE I. The $\mathcal{PT}$ symmetry and the evolution of the energy gap when tuning the gap-control parameter η of the single-spin Hamiltonian under different parametric settings.

	$\delta_x = \delta_y = 0$	$\delta_x = 0, \delta_y \neq 0$	$\delta_x \neq 0, \delta_y = 0$	$\delta_x \neq 0, \delta_y \neq 0$
$\mathcal{PT}$ symmetry	Yes	Yes	No	No
Energy gap of H_0 varies with η	Gap closing	Anticrossing	Anticrossing	Anticrossing

gap between the ground and first excited states [32]. Based on the unique dynamic consequence of EPs discovered here, we propose to detect the gap-closing transition of the nondissipative system through a Landau-Zener-Stückelberg-like process: the system parameters (i.e., the quasimomentum driven by static force for an energy band [30]) are ramped across the $\mathcal{PT}$-symmetry-breaking bubble and then back to the original values. The final state subsequently features equal populations of the two eigenstates when the original Hermitian Hamiltonian experiences gap closing, regardless of the initial state.

The rest of this paper is organized as follows. In Sec. II, we present an analysis of the energy spectra of two-level systems in the presence of spin-dependent dissipations. In Sec. III, we discuss the analytical solutions of the time-evolution equations. The numerical simulations of analytical results in terms of the identification of gap closing are given in Sec. IV. A brief summary is given in Sec. V.

II. SPECTRA OF TWO-LEVEL SYSTEMS WITH $\mathcal{PT}$-SYMMETRIC DISSIPATIONS

We are interested in the dynamics of the two-level system $H = H_0 + H_p$ with the Hermitian model $H_0 = \eta\sigma_z + \delta_x\sigma_x + \delta_y\sigma_y$ and spin-dependent dissipation $H_p = i\gamma\sigma_x$, where η, γ, δ_x, and δ_y are real numbers. With spin rotation around the y axis $\sigma_{x,z} \to \pm\sigma_{z,x}$, the perturbation term becomes proportional to σ_z and can be implemented with state-dependent loss, which has been realized on different platforms [25,33–35]. The experimental implementation is discussed in detail in Appendix B. As the dynamic behaviors of quantum systems in general are associated with their spectral structures, we will first introduce the spectral properties of these non-Hermitian two-level systems in this section.

$\mathcal{PT}$ symmetry is defined as the product of parity symmetry $\mathcal{P} = \sigma_x$ and time-reversal symmetry $\mathcal{T} = i\mathcal{K}\sigma_y$, with $\mathcal{K}$ being the complex-conjugate operator, i.e., $\mathcal{PT} = -\mathcal{K}\sigma_z$. When $\delta_x = 0$, H, H_0, and H_p all possess $\mathcal{PT}$ symmetry, and H describes a generic $\mathcal{PT}$-symmetric model. The two-level nondissipative model shows that a gap-closing transition at $\eta = 0$ is characterized by $H_0 = \eta\sigma_z$ when the gap control parameter η is tuned across the zero point. When the terms σ_x and σ_y are turned on, the nondissipative model shows level anticrossing, although only when $\delta_x = 0$ does the model possess $\mathcal{PT}$ symmetry. The corresponding symmetries and spectral characteristics are summarized in Table I.

As predicted by the perturbation analysis presented in Appendix A, by fixing γ and tuning η, the transitions in $\mathcal{PT}$ symmetry in the eigenstates are observed once H_0 also possesses $\mathcal{PT}$ symmetry, reflected in the transitions between real and imaginary spectra, as exemplified in Fig. 1(a) with $\delta_x = \delta_y = 0$. As discussed in the following, the spectral transition also emerges in another case with $\mathcal{PT}$ symmetry, $\delta_x = 0$ and $\delta_y \neq 0$, but this gives rise to anticrossing rather than gap closing when the dissipative perturbation is absent.

As shown in Fig. 1(a), a $\mathcal{PT}$-symmetry-breaking bubble is observed around $\eta = 0$ in the case where $\delta_x = \delta_y = 0$ (and also in the case with $\delta_x = 0$ and $\delta_y \neq 0$). The expectations of the Pauli matrix σ^z (σ^x) disappear when $\gamma < |\eta|$ ($\gamma > |\eta|$), accompanying the closure of real spectra, although that of σ^y is always finite throughout the phase transition [Fig. 1(b)]. This implies that the threshold for triggering $\mathcal{PT}$-symmetry breaking should be determined by comparing the energy gap between two eigenstates with opposite spin polarizations of H_0 (associated with $\langle\sigma_z\rangle$) and the imaginary perturbation (associated with $\langle\sigma_x\rangle$). This point is consistent with the linear dependence of bubble size on γ, as shown in the inset of Fig. 1(a).

The emergence of the $\mathcal{PT}$-symmetry-breaking bubble can be formally understood with the perturbation theory discussed in Appendix A. The total Hamiltonian $H = H_0 + H_p$ has $\mathcal{PT}$ symmetry $\mathcal{PT} = \mathcal{K}\sigma^z$. For the Hermitian single-spin system H_0, if we set the imaginary σ^x term as a perturbation when $\gamma \ll \eta$, it leads to a second-order correction $\gamma^2/(2\eta)$ $[-\gamma^2/(2\eta)]$ for the lower (upper) nonperturbation eigenvalues of H_0, as we discussed above. On the other hand, when $\eta \ll \gamma$, a second-order correction $i\eta^2/(2\gamma)$ $[-i\eta^2/(2\gamma)]$ is added to the imaginary lower (upper) nonperturbation eigenvalues of H_p by the real σ^z term as a perturbation instead. Approaching the EP points, the energy gap monotonously decreases and finally closes at the EP points to smoothly connect the real and imaginary spectra, although the perturbation conditions gradually become invalid. We would like to note that, again, this is completely different from conventional Hermitian systems, where perturbation coupling between two energy levels

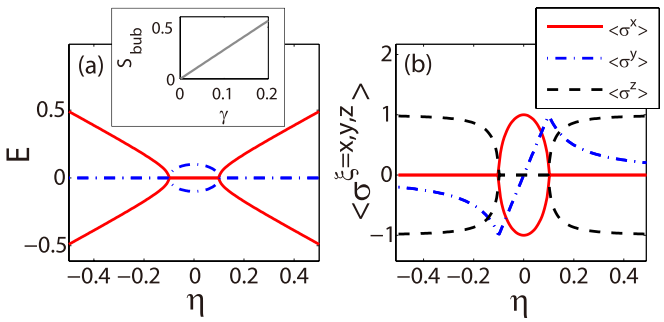

FIG. 1. Illustration of $\mathcal{PT}$-symmetry breaking in the single-spin system H_0. (a) The spectra and (b) spin structure of a single-spin system with $\mathcal{PT}$-symmetry breaking. The red solid (blue dash-dotted) curves in (a) denote the real (imaginary) parts of the spectra. The variation of bubble size (horizontal diameter) with γ is shown in the inset of (a).

usually opens or enlarges a gap rather than leading to gap closing.

It is worth noting that we mainly focus on the microscopic mechanism for the emergence of EPs and imaginary-spectrum bubbles from the point of perturbation theory here [e.g., we answer why the spin-dependent dissipation term leads to the decrease (increase) of the real (imaginary) energy gap], although this phenomenon itself is already known in the community [36–40]. However, previous studies mainly focused on the symmetry protection and topological properties of a nodal line ending with EPs (or EP surfaces enclosing imaginary spectra, i.e., the $\mathcal{PT}$-symmetry-breaking bubble in high dimensions) on energy bands by directly diagonalizing the quasimomentum Hamiltonians of lattice models [36–40].

III. NONADIABATIC TRANSITIONS

The focus of this work is the dynamical time evolution of non-Hermitian Hamiltonians introduced in the previous section. The dynamical process is nonadiabatic, provided the gap control parameters $\eta(t) = \alpha t$ are linearly tuned through the EPs and $\mathcal{PT}$-breaking bubble without a real-energy gap. The observable involved is the asymptotic transition probability between the two levels for $t \to \infty$ in the slow-tuning-speed limit of η, that is, $\alpha \to 0$, which is also called the adiabatic limit [30]. In the absence of a non-Hermitian term, the nonadiabatic transition is reduced to the celebrated Landau-Zener transition of two-level systems.

In a previous work [30], the authors studied the dynamical evolution of a typical $\mathcal{PT}$-symmetric model, $H = \eta\sigma_z + i\gamma\sigma_x$, and predicted that the asymptotic behaviors of the transition probability in the long-time limit $t \to \infty$ would have an equal distribution when η is slowly tuned. In other words, the long-time occupation probabilities of the two levels become the same in the adiabatic limit. It has been shown numerically that the equal-distribution behavior is independent of the initial state. However, a generic $\mathcal{PT}$-symmetric two-level model may include a relevant δ_y term, that is, $H = \eta\sigma_z + \delta_y\sigma_y + i\gamma\sigma_x$, after ignoring the unimportant diagonal term $\delta_0\sigma_0$ [31]. Then it is natural to ask what will happen when the δ_y term is turned on, which drives us to extend the theory developed in Ref. [30].

As shown below, we find that the asymptotic behavior of equal distribution is actually absent for the case with $\delta_y \neq 0$, although the $\mathcal{PT}$ symmetry is preserved and EPs also exist. Instead, the ratio between the final occupation probabilities of the two levels is given by $r_p = |(\gamma - \delta_y)/(\gamma + \delta_y)|$, which is independent of the initial states. It should be noted that the independence of the initial state has been proven only numerically for the case without the δ_y term in the previous work [30]. In contrast, our results prove this point analytically for the generic $\mathcal{PT}$-symmetric model $H = \eta\sigma_z + \delta_y\sigma_y + i\gamma\sigma_x$ here. For comparison, we also briefly discuss the case without $\mathcal{PT}$ symmetry, i.e., when $\delta_x \neq 0$, where the initial state-independent asymptotic behavior is absent.

The route is to solve the time-evolution equation directly with $\eta = \alpha t$. Fortunately, the time-evolution equations of the generic $\mathcal{PT}$-symmetric model $H = \eta\sigma_z + \delta_y\sigma_y + i\gamma\sigma_x$ can be reduced to the celebrated parabolic cylinder equations (Weber equations) [41]. Although the solutions are associated with the complicated confluent hypergeometric functions (Kummer functions), the asymptotic behavior we are concerned with can be obtained with the conclusions derived by a mathematician. In the following, we will discuss the generic $\mathcal{PT}$-symmetric case with $\delta_y \neq 0$ and $\delta_x = 0$ and then discuss the case with $\delta_x \neq 0$ and $\delta_y \neq 0$ without $\mathcal{PT}$ symmetry for comparison.

A. Generic $\mathcal{PT}$-symmetric model: $\delta_y \neq 0$ and $\delta_x = 0$

In this case, the Hamiltonian $H = \eta(t)\sigma_z + \delta_y\sigma_y + i\gamma\sigma_x$ possesses $\mathcal{PT}$ symmetry. As shown in Table I, the energy gap of the Hermitian zeroth-order Hamiltonian $H_0 = \eta(t)\sigma_z + \delta_y\sigma_y$ closes only when $\delta_y = 0$. In general, the level anticrossing appears when $\delta_y \neq 0$ for H_0. But regardless of whether the gap of H_0 closes or not, the loss of initial-state information appears entirely in the presence of a dissipative perturbation.

The two-level model is described by a two-component wave function $\Psi = (\psi_1, \psi_2)^T$. The time-evolution equation of Ψ is given by

$$i\partial_t \begin{pmatrix} \psi_1 \\ \psi_2 \end{pmatrix} = \begin{pmatrix} -\alpha t & i(\gamma - \delta_y) \\ i(\gamma + \delta_y) & \alpha t \end{pmatrix} \begin{pmatrix} \psi_1 \\ \psi_2 \end{pmatrix}. \tag{1}$$

This is a group of coupled first-order differential equations. Fortunately, this equation group can be decoupled by taking the second derivative on the two sides. Specifically, the decoupled second-order differential equation is given by $i\partial_t^2\Psi = (\partial_t H - iH^2)\Psi$, that is,

$$i\partial_t^2\psi_{1,2} = \left\{ \mp\alpha - i\left[(\alpha t)^2 - \left(\gamma^2 - \delta_x^2 - \delta_y^2\right) + 2i\delta_x\gamma\right]\right\}\psi_{1,2}. \tag{2}$$

These equations are actually the standard forms of the parabolic cylinder equations (Weber equations) [41]

$$\frac{d^2\psi_\nu^2}{dz^2} - \left(\frac{1}{4}z^2 + a_\nu\right)\psi_\nu = 0, \quad \nu = 1, 2, \tag{3}$$

with the definition of the new argument $z = e^{-i\pi/4}\sqrt{2\alpha t}$ and constants

$$a_{1,2} = \frac{i\left(\gamma^2 - \delta_y^2\right)}{2\alpha} \mp \frac{1}{2} \tag{4}$$

and can be solved analytically with the confluent hypergeometric functions (i.e., the Kummer functions). In the following, we will first discuss special solutions of Eq. (4). Then a generic solution can be written with the combination of these special solutions. The combination coefficients can be fixed with the initial conditions (i.e., the initial states and the initial first-order derivative of the wave functions). Finally, the asymptotic behaviors of the wave function can be derived with the asymptotic behaviors of the confluent hypergeometric functions. Although the procedure is tedious, the idea is very straightforward.

Before moving to the solutions of the evolution equation, let us first make some comments on the difference from the analysis of the special $\mathcal{PT}$-symmetric model in Ref. [30]. In fact, the forms of the time-evolution equations are all the parabolic cylinder equations shown in Eq. (3). Only the forms of $a_{j=1,2}$ are different, as shown in Eq. (4). According to the theory in [30], this actually implies the nonadiabatic transitions also show equal-distribution asymptotic behavior even for the case with $\delta_y \neq 0$ discussed here. However, we will

show below that the equal-distribution asymptotic behavior is actually absent in the current case, which is also confirmed by our numerics.

The parabolic cylinder equations (3) all have two particular exact symmetric solutions, i.e., the even-parity solution,

$$\begin{aligned} y_{v1} &= e^{-\frac{1}{4}z^2} M\left(\frac{1}{2}a_v + \frac{1}{4}, \frac{1}{2}, \frac{1}{2}z^2\right) \\ &= e^{-\frac{1}{4}z^2}\left\{1 + \left(a_v + \frac{1}{2}\right)\frac{z^2}{2!} + \left(a_v + \frac{1}{2}\right)\left(a_v + \frac{5}{2}\right)\frac{z^2}{2!} \right. \\ &\quad \left. + \cdots\right\}, \end{aligned} \tag{5}$$

and the odd-parity solution,

$$\begin{aligned} y_{v2} &= z e^{-\frac{1}{4}z^2} M\left(\frac{1}{2}a_v + \frac{3}{4}, \frac{3}{2}, \frac{1}{2}z^2\right) \\ &= e^{-\frac{1}{4}z^2}\left\{z + \left(a_v + \frac{3}{2}\right)\frac{z^3}{3!} + \left(a_v + \frac{3}{2}\right)\left(a_v + \frac{7}{2}\right)\frac{z^5}{5!} \right. \\ &\quad \left. + \cdots\right\}, \end{aligned} \tag{6}$$

where the M functions are the confluent hypergeometric functions. Any general solutions of Eq. (1) are superpositions of these two particular solutions, i.e.,

$$\begin{pmatrix} \psi_1 \\ \psi_2 \end{pmatrix} = \begin{pmatrix} \alpha_{11} y_{11} + \alpha_{12} y_{12} \\ \alpha_{21} y_{21} + \alpha_{22} y_{22} \end{pmatrix}. \tag{7}$$

In the next step, we will solve these coefficients with the initial conditions.

The systems are assumed to be prepared in an arbitrary initial state at $t = 0$,

$$\Psi(0) = \begin{pmatrix} \psi_1(0) \\ \psi_2(0) \end{pmatrix} = \begin{pmatrix} A \\ B \end{pmatrix}. \tag{8}$$

Considering $y_1(0) = 1$ and $y_2(0) = 0$, we have $\alpha_{11} = A$ and $\alpha_{21} = B$. The initial conditions of the first-order differential equations give rise to

$$\left.\frac{d}{dz}\Psi(z)\right|_{z=0} = \frac{e^{i\pi/4}}{\sqrt{2\alpha}} \begin{pmatrix} 0 & \gamma - \delta_y \\ \gamma + \delta_y & 0 \end{pmatrix} \begin{pmatrix} A \\ B \end{pmatrix}. \tag{9}$$

It is easy to confirm that $dy_1(0)/dz = 0$ and $dy_2(0)/dz = 1$ from the expansion series in Eqs. (5) and (6). With these conditions, we have

$$\begin{pmatrix} \alpha_{12} \\ \alpha_{22} \end{pmatrix} = \begin{pmatrix} \frac{e^{i\pi/4}}{\sqrt{2\alpha}}(\gamma - \delta_y)B \\ \frac{e^{i\pi/4}}{\sqrt{2\alpha}}(\gamma + \delta_y)A \end{pmatrix}. \tag{10}$$

Therefore, the solutions of the time-evolution equations (1) are given by

$$\Psi = \begin{pmatrix} A y_{11} + \frac{e^{i\pi/4}}{\sqrt{2\alpha}}(\gamma - \delta_y) B y_{12} \\ B y_{21} + \frac{e^{i\pi/4}}{\sqrt{2\alpha}}(\gamma + \delta_y) A y_{22} \end{pmatrix}. \tag{11}$$

We are mainly concerned with the asymptotic behavior in the large-t limit. Our aim is to employ the asymptotic behaviors of the M functions to analyze the asymptotic behaviors of Ψ. Fortunately, the asymptotic behaviors of the confluent hypergeometric functions [41] can be written down as

$$\begin{aligned} \frac{M(a,b,x)}{\Gamma(b)} &= \frac{e^{\pm i\pi a} x^{-a}}{\Gamma(b-a)} \left\{ \sum_{n=0}^{R-1} \frac{(a)_n (1 + a - b)_n}{n!} (-x)^{-n} \right. \\ &\quad \left. + O(|x|^{-R}) \right\} + \frac{e^x x^{a-b}}{\Gamma(a)} \left\{ \sum_{n=0}^{S-1} \frac{(b-a)_n (1-a)_n}{n!} x^{-n} \right. \\ &\quad \left. \times O(|x|^{-S}) \right\} \end{aligned} \tag{12}$$

when $|x| \to \infty$, where

$$(f)_n = f(f+1)(f+2)\cdots(f+n-1), (f)_0 = 1. \tag{13}$$

The signs $\pm$ correspond to the argument of x in the ranges $-\frac{1}{2}\pi < \arg(x) < \frac{3}{2}\pi$ and $-\frac{3}{2}\pi < \arg(x) \leqslant -\frac{1}{2}\pi$, respectively.

Now let us discuss the leading-order terms for the asymptotic behaviors of the generic solutions in Eqs. (7). From Eqs. (5) and (6), we find that y_1 and y_2 involve different coefficients a and b but the same argument $x = z^2/2$ appearing in Eq. (12). Since $\arg(z^2/2) = -\pi/2$, we always need to take the minus sign in Eq. (12). The leading-order terms of the y functions are determined by the magnitudes of $-a$ and $(a - b)$ since only the zeroth-order terms of the expansion series in Eq. (12) need to be considered. The values of $-a$ and $(a - b)$ are listed in Table II. It is shown that, for y_{11} and y_{12} (y_{21} and y_{22}), the first terms with power $-a$ [the second terms with power $(a - b)$] in Eq. (12) are dominant. Relative to y_{11} and y_{21}, although y_{12} and y_{22} have an additional x argument before the M function from Eqs. (5) and (6), they are counteracted by the real parts of $-a$ and $(a - b)$. Therefore, the asymptotic behaviors of the y functions are all proportional zeroth-order

TABLE II. The values of $-a$ and $(a - b)$ for different y functions.

	a	b	$-a$	$a - b$
y_{11}	$\frac{1}{2}a_1 + \frac{1}{4}$	$\frac{1}{2}$	$-\frac{i(\gamma^2 - \delta_y^2)}{4\alpha}$	$\frac{i(\gamma^2 - \delta_y^2)}{4\alpha} - \frac{1}{2}$
y_{12}	$\frac{1}{2}a_1 + \frac{3}{4}$	$\frac{3}{2}$	$-\frac{i(\gamma^2 - \delta_y^2)}{4\alpha} - \frac{1}{2}$	$\frac{i(\gamma^2 - \delta_y^2)}{4\alpha} - 1$
y_{21}	$\frac{1}{2}a_2 + \frac{1}{4}$	$\frac{1}{2}$	$-\frac{i(\gamma^2 - \delta_y^2)}{4\alpha} - \frac{1}{2}$	$\frac{i(\gamma^2 - \delta_y^2)}{4\alpha}$
y_{22}	$\frac{1}{2}a_2 + \frac{3}{4}$	$\frac{3}{2}$	$-\frac{i(\gamma^2 - \delta_y^2)}{4\alpha} - 1$	$\frac{i(\gamma^2 - \delta_y^2)}{4\alpha} - \frac{1}{2}$

terms of z, which are given by

$$y_{11}\sim e^{-\frac{1}{4}x^2}\frac{\Gamma\left(\frac{1}{2}\right)e^{\pi(\gamma^2-\delta_y^2)/4\alpha}}{\Gamma\left(\frac{1}{2}-\frac{i(\gamma^2-\delta_y^2)}{4\alpha}\right)}\left(\frac{x^2}{2}\right)^{-i(\gamma^2-\delta_y^2)/4\alpha},\quad y_{12}\sim -ie^{-\frac{1}{4}x^2}\frac{\sqrt{2}\Gamma\left(\frac{3}{2}\right)e^{\pi(\gamma^2-\delta_y^2)/4\alpha}}{\Gamma\left(1-\frac{i(\gamma^2-\delta_y^2)}{4\alpha}\right)}\left(\frac{x^2}{2}\right)^{-i(\gamma^2-\delta_y^2)/4\alpha},$$
$$y_{21}\sim e^{\frac{1}{4}x^2}\frac{\Gamma\left(\frac{1}{2}\right)}{\Gamma\left(\frac{1}{2}+\frac{i(\gamma^2-\delta_y^2)}{4\alpha}\right)}\left(\frac{x^2}{2}\right)^{i(\gamma^2-\delta_y^2)/4\alpha},\quad y_{22}\sim e^{\frac{1}{4}x^2}\frac{\sqrt{2}\Gamma\left(\frac{3}{2}\right)}{\Gamma\left(1+\frac{i(\gamma^2-\delta_y^2)}{4\alpha}\right)}\left(\frac{x^2}{2}\right)^{i(\gamma^2-\delta_y^2)/4\alpha}. \tag{14}$$

Further, by substituting the expressions in Eq. (14) into Eq. (11), we get

$$\frac{\psi_1}{\psi_2}\sim e^{\pi(\gamma^2-\delta_y^2)/4\alpha}\left(\frac{z^2}{2}\right)^{-\frac{i(\gamma^2-\delta_y^2)}{2\alpha}}\left[A\frac{\Gamma\left(\frac{1}{2}\right)}{\Gamma\left(\frac{1}{2}-\frac{i(\gamma^2-\delta_y^2)}{4\alpha}\right)}+Be^{-i\pi/4}\frac{\gamma-\delta_y}{\sqrt{\alpha}}\frac{\Gamma\left(\frac{3}{2}\right)}{\Gamma\left(1-\frac{i(\gamma^2-\delta_y^2)}{4\alpha}\right)}\right]$$
$$\div\left[B\frac{\Gamma\left(\frac{1}{2}\right)}{\Gamma\left(\frac{1}{2}+\frac{i(\gamma^2-\delta_y^2)}{4\alpha}\right)}+Ae^{i\pi/4}\frac{\gamma+\delta_y}{\sqrt{\alpha}}\frac{\Gamma\left(\frac{3}{2}\right)}{\Gamma\left(1+\frac{i(\gamma^2-\delta_y^2)}{4\alpha}\right)}\right]. \tag{15}$$

By defining $\tilde{\gamma}^2=(\gamma^2-\delta_y^2)/\alpha$ and considering $\Gamma(1/2)=2\Gamma(3/2)$, we have

$$\left|\frac{\psi_1}{\psi_2}\right|\sim\frac{e^{\pi\frac{\tilde{\gamma}^2}{4}}\left|\left(\frac{z^2}{2}\right)^{-\frac{i\tilde{\gamma}^2}{2}}\right|\left|\frac{2A}{\Gamma\left(\frac{1}{2}-\frac{i\tilde{\gamma}^2}{4}\right)}+\frac{\gamma-\delta_y}{\sqrt{\alpha}}\frac{e^{-i\pi/4}B}{\Gamma\left(1-\frac{i\tilde{\gamma}^2}{4}\right)}\right|}{\left|\frac{2B}{\Gamma\left(\frac{1}{2}+\frac{i\tilde{\gamma}^2}{4}\right)}+\frac{\gamma+\delta_y}{\sqrt{\alpha}}\frac{e^{i\pi/4}A}{\Gamma\left(1+\frac{i\tilde{\gamma}^2}{4}\right)}\right|}$$
$$=\left|\frac{2\sqrt{\alpha}\Gamma\left(1+\frac{i\tilde{\gamma}^2}{4}\right)e^{\pi\frac{\tilde{\gamma}^2}{4}}\left(\frac{z^2}{2}\right)^{-\frac{i\tilde{\gamma}^2}{2}}}{(\gamma+\delta_y)\Gamma\left(\frac{1}{2}-\frac{i\tilde{\gamma}^2}{4}\right)}\right|$$
$$\times\left|\frac{A+Be^{-i\pi/4}\frac{\gamma-\delta_y}{2\sqrt{\alpha}}\frac{\Gamma\left(\frac{1}{2}-\frac{i\tilde{\gamma}^2}{4}\right)}{\Gamma\left(1-\frac{i\tilde{\gamma}^2}{4}\right)}}{A+Be^{-i\pi/4}\frac{2\sqrt{\alpha}}{\gamma+\delta_y}\frac{\Gamma\left(1+\frac{i\tilde{\gamma}^2}{4}\right)}{\Gamma\left(\frac{1}{2}+\frac{i\tilde{\gamma}^2}{4}\right)}}\right|. \tag{16}$$

Since $\Gamma(\xi)=\int_0^\infty d\tau\,\tau^{\xi-1}e^{-\tau}$, $\Gamma(\xi)^*=\Gamma(\xi^*)$, and then the ratio between the coefficients before B in the above equation is given by

$$\frac{\tilde{\gamma}^2}{4}\frac{\Gamma\left(\frac{1}{2}-\frac{i\tilde{\gamma}^2}{4}\right)\Gamma\left(\frac{1}{2}+\frac{i\tilde{\gamma}^2}{4}\right)}{\Gamma\left(1-\frac{i\tilde{\gamma}^2}{4}\right)\Gamma\left(1+\frac{i\tilde{\gamma}^2}{4}\right)}=\frac{\tilde{\gamma}^2}{4}\frac{\left|\Gamma\left(\frac{1}{2}+\frac{i\tilde{\gamma}^2}{4}\right)\right|^2}{\left|\Gamma\left(1+\frac{i\tilde{\gamma}^2}{4}\right)\right|^2}. \tag{17}$$

Further, by employing the properties of the Γ function,

$$\left|\Gamma\left(\frac{1}{2}+\lambda i\right)\right|^2=\frac{\pi}{\cosh(\pi\lambda)},\quad |\Gamma(1+\lambda i)|^2=\frac{\pi\lambda}{\sinh(\pi\lambda)}, \tag{18}$$

the above equation can be rewritten as

$$\frac{\tilde{\gamma}^2}{4}\frac{\left|\Gamma\left(\frac{1}{2}+\frac{i\tilde{\gamma}^2}{4}\right)\right|^2}{\left|\Gamma\left(1+\frac{i\tilde{\gamma}^2}{4}\right)\right|^2}=\tanh\left(\pi\frac{\tilde{\gamma}^2}{4}\right). \tag{19}$$

In the adiabatic limit $\tilde{\gamma}^2\to\infty$, this ratio becomes 1. Thus, we finally have

$$\lim_{\tilde{\gamma}\to\infty}\left|\frac{\psi_1}{\psi_2}\right|\sim\lim_{\tilde{\gamma}\to\infty}\left|\frac{2\sqrt{\alpha}\Gamma\left(1+\frac{i\tilde{\gamma}^2}{4}\right)e^{\pi\frac{\tilde{\gamma}^2}{4}}\left(\frac{z^2}{2}\right)^{-\frac{i\tilde{\gamma}^2}{2}}}{(\gamma+\delta_y)\Gamma\left(\frac{1}{2}-\frac{i\tilde{\gamma}^2}{4}\right)}\right|$$
$$=\lim_{\tilde{\gamma}\to\infty}\left|\frac{2\sqrt{\alpha}}{\gamma+\delta_y}e^{\pi\frac{\tilde{\gamma}^2}{4}}\left(e^{-i\frac{\pi}{2}}\frac{|z|^2}{2}\right)^{-\frac{i\tilde{\gamma}^2}{2}}\right|$$
$$\times\left|\frac{\tilde{\gamma}^2}{4\tanh(\pi\tilde{\gamma}^2/4)}\right|^{1/2}=\left|\frac{\gamma-\delta_y}{\gamma+\delta_y}\right|^{1/2}. \tag{20}$$

This proves that the ratio between the occupation probabilities of the two states is a constant, $r_p=|(\gamma-\delta_y)/(\gamma+\delta_y)|$, which is independent of the initial states. In addition, only when $\delta_y=0$ does $r_p=1$, which proves the equal-distribution asymptotic behavior elaborated at the beginning of this section. Although the $\mathcal{PT}$-symmetry-breaking bubble also emerges for finite δ_y, the equal-distribution asymptotic behavior does not exist in this case.

B. Case without $\mathcal{PT}$ symmetry: $\delta_y\neq 0$ and $\delta_x\neq 0$

When $\delta_x\neq 0$, regardless of whether δ_y is finite or not, the $\mathcal{PT}$ symmetry is absent. We study this case just for comparison. In this case, the time-evolution equation is given by

$$i\partial_t\begin{pmatrix}\psi_1\\ \psi_2\end{pmatrix}=\begin{pmatrix}-\alpha t & \delta_x+i(\gamma-\delta_y)\\ \delta_x+i(\gamma+\delta_y) & \alpha t\end{pmatrix}\begin{pmatrix}\psi_1\\ \psi_2\end{pmatrix}. \tag{21}$$

The second-order differential equation takes the form

$$i\partial_t^2\psi_{1,2}=\left\{\mp\alpha-i\left[(\alpha t)^2-\left(\gamma^2-\delta_x^2-\delta_y^2\right)+2i\delta_x\gamma\right]\right\}\psi_{1,2}, \tag{22}$$

which corresponds to the parabolic cylinder equation

$$\frac{d^2\psi_\xi^2}{dz^2}-\left(\frac{1}{4}z^2+a_\xi\right)\psi_\xi=0,\quad \xi=1,2, \tag{23}$$

with

$$a_{1,2} = \frac{i\left(\gamma^2 - \delta_x^2 - \delta_y^2\right) + 2\delta_x\gamma}{2\alpha} \mp \frac{1}{2}. \tag{24}$$

The only difference is the form of the a factor.

For simplicity, we take the special initial state $\Psi(0) = (0 \quad 1)^T$ as an example. Like in the previous section, with these initial conditions, it gives rise to the solution

$$\Psi = \begin{pmatrix} e^{-i\pi/4}\frac{\delta_x + i(\gamma - \delta_y)}{\sqrt{2\alpha}} y_{12} \\ y_{21} \end{pmatrix}$$
$$= e^{-\frac{1}{4}z^2}\begin{pmatrix} e^{-i\pi/4}\frac{\delta_x + i(\gamma - \delta_y)}{\sqrt{2\alpha}} z M(\frac{1}{2}a_1 + \frac{3}{4}, \frac{3}{2}, \frac{1}{2}z^2) \\ M(\frac{1}{2}a_2 + \frac{1}{4}, \frac{1}{2}, \frac{1}{2}z^2) \end{pmatrix}. \tag{25}$$

In the limit $z \to \infty$, for ψ_1, because

$$-a = -\left(\frac{a_1}{2} + \frac{3}{4}\right) = -\frac{1}{2} - \frac{i\left(\gamma^2 - \delta_y^2 - \delta_x^2\right) + 2\delta_x\delta_y}{4\alpha},$$
$$a - b = \frac{a_1}{2} - \frac{3}{4} = -1 + \frac{i\left(\gamma^2 - \delta_y^2 - \delta_x^2\right) + 2\delta_x\delta_y}{4\alpha} \tag{26}$$

have large real parts $\delta_x\delta_y/\alpha$ in the adiabatic limit, we need to compare their real parts in order to determine the dominant terms in the asymptotic expansion of the M functions [see Eq. (12)]. This can be divided into two cases; when $\delta_y\delta_x/\alpha < 0.5$, the first term in Eq. (12) is dominant, and when $\delta_y\delta_x/\alpha > 0.5$, the second term becomes dominant. For ψ_2, similarly, we have

$$-a = -\left(\frac{a_2}{2} + \frac{1}{4}\right) = -\frac{1}{2} - \frac{i\left(\gamma^2 - \delta_y^2 - \delta_x^2\right) + 2\delta_x\delta_y}{4\alpha},$$
$$a - b = \frac{a_2}{2} - \frac{1}{4} = \frac{i\left(\gamma^2 - \delta_y^2 - \delta_x^2\right) + 2\delta_x\delta_y}{4\alpha}. \tag{27}$$

When $\delta_y\delta_x/\alpha < -0.5$, the first term in the asymptotic expansion is dominant, but when $\delta_y\delta_x/\alpha > -0.5$, the second term becomes dominant. These results are reasonable because the EPs are absent when $\delta_x \neq 0$ and the two levels always have a gap when η is tuned, and thus, the time evolution becomes adiabatic in the slow-tuning-speed limit.

In summary, when $\delta_y\delta_x/\alpha < -0.5$, by defining

$$\epsilon = \frac{i\left(\gamma^2 - \delta_y^2 - \delta_x^2\right) + 2\delta_x\delta_y}{4\alpha}, \tag{28}$$

we have

$$M\left(\frac{1}{2}a_1 + \frac{3}{4}, \frac{3}{2}, \frac{1}{2}z^2\right) = \frac{\Gamma(\frac{3}{2})e^{-i\pi(\frac{1}{2}+\epsilon)}(\frac{z^2}{2})^{-(\frac{1}{2}+\epsilon)}}{\Gamma(1-\epsilon)},$$
$$M\left(\frac{1}{2}a_2 + \frac{1}{4}, \frac{1}{2}, \frac{1}{2}z^2\right) = \frac{\Gamma(\frac{1}{2})e^{-i\pi(\frac{1}{2}+\epsilon)}(\frac{z^2}{2})^{-(\frac{1}{2}+\epsilon)}}{\Gamma(-\epsilon)}, \tag{29}$$

which implies $\psi_1 \propto z^{-2\epsilon}$ and $\psi_1 \propto z^{-1-2\epsilon}$ and thus $|\frac{\psi_1}{\psi_2}|^2 \propto z^2 \to \infty$. Similarly, when $-0.5 < \delta_y\delta_x/\alpha < 0.5$, $\psi_1 \propto z^{-2\epsilon}$, and $\psi_1 \propto z^{-2\epsilon}$, which implies that only when $\delta_y\delta_z = 0$ is it possible to get $|\frac{\psi_1}{\psi_2}|^2 \to 1$. As we showed in the previous section, actually, only when $\delta_y = \delta_z = 0$ do we have this result, i.e., the equal-distribution asymptotic behavior. For the case with $\delta_y\delta_x/\alpha > 0.5$, we have $\psi_1 \propto z^{-2-2\epsilon}$ and $\psi_1 \propto z^{2\epsilon}$, and $|\frac{\psi_1}{\psi_2}|^2$ also cannot give rise to the equal-distribution asymptotic behavior.

Therefore, although the $\mathcal{PT}$ symmetry and the initial-state-independent asymptotic behavior are both preserved when $\delta_y \neq 0$, the equal-distribution asymptotic behavior disappears. In contrast, only when $\delta_x = \delta_y = 0$ do the nonadiabatic transitions show the equal-distribution asymptotic behavior. When $\delta_x \neq 0$, we have adiabatic transitions because the EPs are absent. These are the main conclusions of this article.

For H_0, only when $\delta_x = \delta_y = 0$ does the variation of η give rise to the gap-closing transition. If δ_x or δ_y becomes finite, the gap closing is replaced by an anticrossing of the two levels. Therefore, the equal-distribution asymptotic behavior may be employed as a way to identify gap closing. We will show the numerical simulations in terms of this application below.

IV. IDENTIFICATION OF GAP CLOSING WITH THE DYNAMICAL METHOD

As shown above, we find the equal-distribution behavior is present when the nondissipative Hamiltonian has a gap-closing transition and disappears when the nondissipative Hamiltonian displays level anticrossing even when the $\mathcal{PT}$ symmetry and thus EPs are still present. By employing these unique properties, we propose to identify the energy gap closing in the nondissipative Hamiltonian with a cyclic time evolution covering the $\mathcal{PT}$-symmetry-breaking bubble, mimicking Landau-Zener-Stückelberg interference [42]. It can be implemented by driving particles on the Bloch bands through a static force [30,42]. Specifically, we propose to start from a parametric point, e.g., $\eta = -1$, and tune η across the $\mathcal{PT}$-symmetry-breaking bubble at around $\eta = 0$ and back to the start point $\eta = -1$. By observing the projection probabilities of the final state for the instantaneous ground and excited states, which are connected to the states that coalesce at the EPs, we can gain the signature of the gap closing. As long as the tuning speed is slow enough, we can observe almost equal projection probabilities when H_0 indeed experiences a gap-closing transition.

The instantaneous projection probabilities and spectra (insets) of the cyclic time evolution [$\eta(t) = -1 + \alpha t$ when $t < t_f$ and $\eta(t) = 1 - \alpha t$ when $t > t_f$, with $\alpha = 1/15$] are shown in Fig. 2 for different parameters (all with arbitrary units in this paper). The top and bottom rows of Fig. 2 show the cases without and with dissipative perturbations. The plots from left to right correspond to the Hamiltonians $H_0 = \eta(t)\sigma_z$, $\eta(t)\sigma_z + \delta_x\sigma_x$, and $\eta(t)\sigma_z + \delta_y\sigma_y$ (i.e., $H = \eta(t)\sigma_z + i\gamma\sigma_x$, $\eta(t)\sigma_z + \delta_x\sigma_x + i\gamma\sigma_x$, and $\eta(t)\sigma_z + \delta_y\sigma_y + i\gamma\sigma_x$), respectively. The initial state is prepared as an arbitrary superposition of the eigenstates of the lower and higher levels at $t = 0$. As shown in Fig. 2(a), where $H = H_0 = \eta(t)\sigma_z$, the instantaneous state has invariant projection probabilities for the eigenstates, although the spectra show a gap closing. That is because there is no coupling between the ground and excited states. When the imaginary perturbation is present, i.e., $H = H_0 + H_p = \eta(t)\sigma_z + i\gamma H_p$, where a the $\mathcal{PT}$-symmetry-breaking bubble emerges at around the gap-closing point [see the inset of Fig. 2(d)], the instantaneous projection probabilities for the two levels take almost the same instantaneous values after

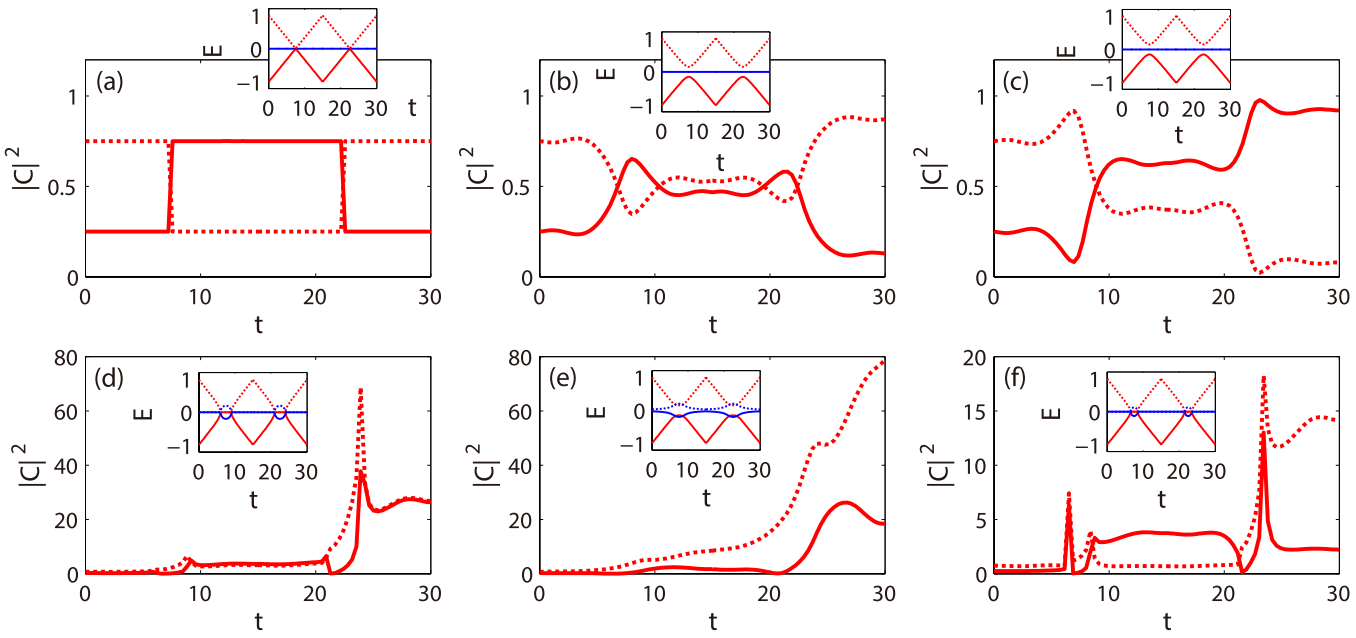

FIG. 2. The illustration of instantaneous spectra (top row) and projection properties (bottom row) for different perturbation parameters in a cyclic time evolution, where $\eta(t) = -1 + \alpha t$ when $t < t_f$ and $\eta(t) = 1 - \alpha t$ when $t > t_f$ with the one-way evolution time $t_f = 15$ and tuning speed $\alpha = 0.025$. The initial states are taken as $|\Psi(0)\rangle = \cos(\theta)|\Psi_1(0)\rangle + e^{i\varphi}\sin(\theta)|\Psi_2(0)\rangle$, with $\theta = \pi/3$ and $\varphi = \pi/6$, where $|\Psi_{1,2}(0)\rangle$ are the instantaneous eigenstates at moment $t = 0$. The spectra of the real-time Hamiltonian $H = \eta(t)\sigma_z + \delta_x\sigma_x + \delta_y\sigma_y + i\gamma\sigma_x$ (insets) and the projection probabilities of instantaneous states when (a) $\gamma = \delta_x = \delta_y = 0$ [(d) $\delta_y = \delta_x = 0$, $\gamma = 0.2$], (b) $\gamma = \delta_y = 0$, $\delta_x = 0.15$ [(e) $\delta_y = 0$, $\delta_x = 0.15$, $\gamma = 0.2$], and (c) $\gamma = \delta_x = 0$, $\delta_y = 0.15$ [(f) $\delta_x = 0$, $\delta_y = 0.15$, $\gamma = 0.2$], are shown. The red (blue) curves in the insets represent the real (imaginary) parts of the spectra. The solid (dotted) curves in the main plots show the projection probabilities for the corresponding levels in the insets. The projection probabilities $|C_{\xi=1,2}|^2$ are defined as $C_{1,2} = \langle\tilde{\Psi}_{1,2}(t)|\Psi(t)\rangle/|\langle\tilde{\Psi}_{1,2}|\Psi_{1,2}\rangle|$, with $|\Psi(t)\rangle$ being the instantaneous state and $|\Psi_{1,2}(t)\rangle$ [$|\tilde{\Psi}_{1,2}(t)\rangle$] being the instantaneous right (left) eigenstates [43]. We would like to note that the coefficients $C_{1,2}$ are not the spin components directly. However, because η is far larger than other coefficients in the Hamiltonian at $t = t_f$, $\Psi_{1,2}$ approach the eigenstate of σ_z. Therefore, the asymptotic behaviors of $C_{1,2}$ approach those of $\psi_{1,2}$ given in Sec. III. The introduction of $C_{1,2}$ is just for the convenience of experimental observation.

passing the EPs [see Fig. 2(d)]. This is a good signature for probing the gap-closing transition in the original Hamiltonian H_0.

Let us further discuss the cases where the gap closing in H_0 is absent. Following Figs. 2(a) and 2(d), a real-spin term $\delta_x\sigma^x$ is introduced in Figs. 2(b) and 2(e). This real-spin term prevents the gap closing at $\eta = 0$ and leads to anticrossing at around $\eta = 0$. In addition, it also breaks the $\mathcal{PT}$ symmetry because $\mathcal{K}\sigma^z\sigma^x\sigma^z\mathcal{K}^\dagger = -\sigma^x$, as discussed above. Figure 2(b), where the imaginary perturbation is not turned on, shows the spectra indeed have a finite gap when $\eta = 0$ (see the inset). The finite real-energy gap allows the Landau-Zener tunneling from the lower level to the higher level, and the instantaneous projection probabilities are distributed unequally. When the time evolution tends to the adiabatic limit $\delta_x^2/\alpha \gg 1$ (here $\delta_x^2/\alpha \sim 0.34$), the projection probabilities should remain constant as the energy gap completely suppresses the tunneling. Due to the absence of $\mathcal{PT}$ symmetry, the spectra in the case with imaginary perturbation [see inset of Fig. 2(e)] always have imaginary parts, and the instantaneous projection probability of the level with positive imaginary spectra is amplified after long-time evolution and becomes dominant.

In Figs. 2(c) and 2(f), another kind of real term, $\delta_y\sigma^y$, is introduced in H_0 to break the gap closing. This perturbation also opens a finite gap at $\eta = 0$ and thus leads to anticrossing as well. But unlike in Figs. 2(b) and 2(e), the $\mathcal{PT}$ symmetry is still preserved in this case since $\mathcal{K}\sigma^z\sigma^y\sigma^z\mathcal{K}^\dagger = \sigma^y$. The behaviors of the time evolution in the case without imaginary perturbation look like the case with the δ_x term [see Fig. 2(c)]. When the time evolution tends to the adiabatic limit $\delta_y^2/\alpha \gg 1$, the projection probabilities should also remain constant, although it is not in this limit here because $\delta_y^2/\alpha \sim 0.34$. The fluctuations in the projection probabilities in Fig. 2 are due to the Landau-Zener tunneling for nonadiabatic evolution. What we want to emphasize is that, although the energy gap closes and a $\mathcal{PT}$-symmetry-breaking bubble emerges when the imaginary perturbation is turned on and is large enough, i.e., $\gamma > \delta_y$ [see the inset of Fig. 2(f); note that the gap is still open when $\gamma < \delta_y$], because the $\mathcal{PT}$ symmetry is preserved in both H_0 and H, the projection probabilities do not show the equality like in the case with gap closing in Fig. 2(d). This observation was not reported previously since only the cases without the σ_y term were discussed [30]. Therefore, the equality of asymptotic instantaneous projection probabilities can be observed only in the case where H_0 has a gap-closing transition when the dissipative perturbation is turned on and can be employed as a unique signature of gap closing in H_0.

However, the analysis in Ref. [30] showed that the equality of projection probabilities survives under the adiabatic

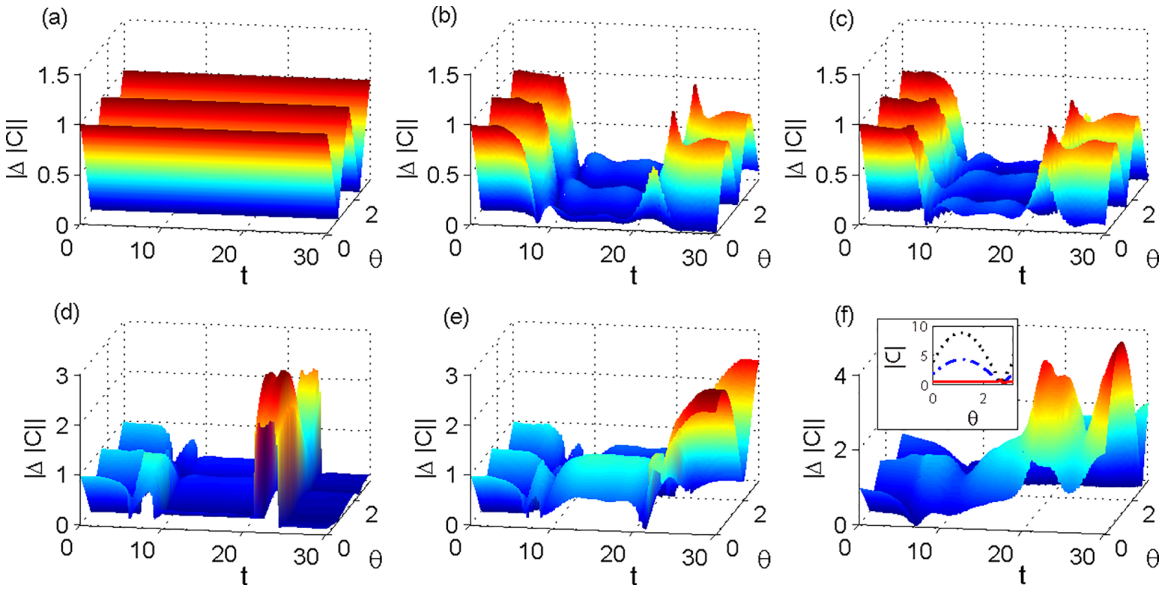

FIG. 3. The difference between the probability amplitudes $|\Delta|C|| = ||C_2| - |C_1||$ for different initial states in cyclic evolution. The initial states are taken as $|\Psi(0)\rangle = \cos(\theta)|\Psi_1(0)\rangle + e^{i\varphi}\sin(\theta)|\Psi_2(0)\rangle$, where φ is arbitrarily fixed at $\pi/6$ and θ is scanned. These plots have the same parameters as the corresponding plots in Fig. 2. The inset of (f) shows $|C_1|$ (blue dash-dotted line), $|C_2|$ (black dotted line), and their ratio $|C_2|/|C_1|$ (red solid line) at $t = t_f$. The ratio remains constant except around the zero point of C, which confirms the analytical result that the independence of the initial states is preserved as long as the system crosses EPs.

condition $\gamma^2/\alpha \gg 1$ for the model $H = \eta\sigma_z + i\gamma\sigma_x$, where α is the tuning speed of η, the same as our model in Fig. 2(d). In order to mimic a realistic situation where the adiabaticity may be hard to satisfy, we take $t_f = 15$ and thus $\gamma^2/\alpha \sim 0.6$ here. We would like to note that, even in this case, as shown in Fig. 2, the nonadiabatic transition shows almost perfect coincidence in the projection probabilities of the final instantaneous states for the two levels. This implies that this phenomenon is not strongly dependent on the adiabatic condition. Another point that needs to be noted is that our models actually neglect the background loss term which usually exists in experiment, and thus, the probabilities become larger than 1. The background loss term is proportional to γ and leads to a scaling of $\exp(-2\gamma t_f) \sim 1/400$ in the final probabilities. This means the effective final probabilities are about $20/400 = 5\%$ in Fig. 2(d). We will lose about 95% of the particles in the experiment.

The presence of equal redistribution is also independent of the preparation of the initial state. In Fig. 3 , the differences between the instantaneous projection amplitudes are shown for different initial states. From Fig. 3, we can see that the differences between the instantaneous projection probabilities are almost nonexistent for all initial states in the case with gap closing. In contrast, the final probability differences are not vanishing and vary for different initial states in all other cases (including the case with both anticrossing and $\mathcal{PT}$ symmetry and that with anticrossing but without $\mathcal{PT}$ symmetry), as discussed in Fig. 2. This implies we do not need to determine a special initial state to identify the gap-closing transition in the experiment.

From the above discussions, the proposed scheme can be expanded in the following steps. In order to identify the gap closing in a system, we first need to introduce a dissipative perturbation that is noncommutative with the original (zeroth-order) Hermitian Hamiltonian. Second, we need to tune the parameter, which may lead to gap closing or anticrossing along a cyclic trajectory covering the possible critical point and observe the projection probabilities of the final states to check whether the equal redistribution occurs. If the system always has a small gap, i.e., shows anticrossing behavior, rather than true gap closing, the equal redistribution will be broken. With these steps, we can identify whether the system indeed has a gap-closing transition. We do not need to tune the parameter precisely to the gap-closing point and elaborate the initial states, which are usually required in a conventional scheme. This provides us a paradigm for using dissipation in metrology.

V. CONCLUSION

In summary, we systematically characterized the nonadiabatic transitions of a generic non-Hermitian $\mathcal{PT}$-symmetric two-level model. The time evolution crossing the EPs shows initial-state-independent asymptotic behaviors. Particularly, only when the nondissipative Hamiltonian shows gap closing are the asymptotic probabilities of particles on the two levels the same in the slow-tuning-speed limit. Equal redistribution is absent when the nondissipative Hamiltonian displays level anticrossing. As long as EPs are crossed, the ratio between the asymptotic probabilities is initial state independent. We thus further propose to identify gap closing with dissipative dynamics in Hermitian systems. Our proposal should be able to be checked with techniques shown in current experiments [25,33–35], as exemplified in Appendix B. For example, the extension of the dynamical evolution encircling EPs in atomic

gases to that crossing EPs is possible [25]. It is worth noting that the idea presented here is also essentially different from the proposal to identify exceptional points with quench dynamics [44].

ACKNOWLEDGMENTS

The authors wish to thank Prof. W. Yi, Prof. Z.-B. Yang, and Prof. S.-B. Zheng for very helpful discussions and also thank Prof. W. Yi for suggestions on writing. J.-S.P. is supported by the National Natural Science Foundation of China (Grant No. 11904228) and the Science Specialty Program of Sichuan University (Grant No. 2020SCUNL210). F.W. is supported by the National Youth Science Foundation of China (CN; Grant No. 12204105), the Educational Research Project for Young and Middle-Aged Teachers of Fujian Province (CN; Grant No. JAT210041), and the Natural Science Foundation of Fujian Province (CN; Grant No. 2022J05116).

APPENDIX A: DISSIPATIVE PERTURBATION

We present the perturbation analysis of the impact of dissipative perturbation on a gap-closing transition or level anticrossing in this Appendix. Gap closing or anticrossing typically involves two states, the ground state $|\Psi_g\rangle$ and the excited state $|\Psi_e\rangle$, which approach and move away from each other when coupling strength η is tuned. We assume the original Hamiltonian $H_0(\eta)$ is perturbed by a dissipative perturbation $H_p = \mathrm{i}\lambda V_p$, with V_p being a Hermitian Hamiltonian and λ being a small parameter, which generally can be implemented with state-dependent loss in experiment [25,33]. We assume H_0, H_p, and the total Hamiltonian $H = H_0 + H_p$ possess the product of parity ($\mathcal{P}$) and time-reversal ($\mathcal{T}$) symmetries, i.e., the so-called $\mathcal{PT}$ symmetry: $\mathcal{PT}H_0(\mathcal{PT})^{-1} = H_0$, $\mathcal{PT}H_p(\mathcal{PT})^{-1} = H_p$ and $\mathcal{PT}H(\mathcal{PT})^{-1} = H$. Without loss of generality, we also assume H_0 does not commutate with H_p, and thus, H_p perturbatively mixes the eigenstates of H_0.

Let us employ perturbation theory to analyze the impact of H_p on the spectra of H_0. Specifically, for the zero-order eigenstates $|\Psi_\xi\rangle$ and eigenvalues E_ξ, which satisfy $H_0|\Psi_\xi\rangle = E_\xi|\Psi_\xi\rangle$, the perturbation expansion of the Schrodinger equation is given by

$$\begin{aligned}(H_0 + \mathrm{i}\lambda V_p)(|\Psi_\xi\rangle + |\Psi_\xi^{(1)}\rangle + \cdots) \\ = (E_\lambda + E_\xi^{(1)} + \cdots)(|\Psi_\xi\rangle + |\Psi_\xi^{(1)}\rangle + \cdots),\end{aligned} \tag{A1}$$

where $|\Psi_\xi^{(n)}\rangle$ and $E_\xi^{(n)}$ are the nth-order corrections of the eigenstates and eigenenergies. It is worth noting that our unperturbed Hamiltonian is Hermitian. It is essentially different from the perturbation theory of a non-Hermitian Hamiltonian [45], where the zeroth-order basis is defined in the framework of biorthogonal theory [43]. By matching order by order, we derive

$$\begin{aligned}H_0|\Psi_\xi\rangle &= E_\xi|\Psi_\xi\rangle, \\ H_0|\Psi_\xi^{(1)}\rangle + \mathrm{i}\lambda V_p|\Psi_\xi\rangle &= E_\xi|\Psi_\xi^{(1)}\rangle + E_\xi^{(1)}|\Psi_\xi\rangle, \\ &\cdots .\end{aligned} \tag{A2}$$

Multiplying $\langle\Psi_\xi|$ from the left, we derive $E_\xi^{(1)} = \mathrm{i}\lambda\langle\Psi_\xi|V_p|\Psi_\xi\rangle$, as $\langle\Psi_\xi|\Psi_\xi^{(1)}\rangle = 0$.

By noting that $\mathcal{PT}iV_p(\mathcal{PT})^{-1} = -i\mathcal{PT}V_p(\mathcal{PT})^{-1} = iV_p$, we derive $\mathcal{PT}V_p(\mathcal{PT})^{-1} = -V_p$. On the other hand, $\mathcal{PT}H_0(\mathcal{PT})^{-1} = H_0$, and thus, $\mathcal{PT}H_0|\Psi_\xi\rangle = H_0(\mathcal{PT}|\Psi_\xi\rangle = E(\mathcal{PT}|\Psi_\xi\rangle)$. It follows that $\mathcal{PT}|\Psi_\xi\rangle = e^{i\phi}|\Psi_\xi\rangle$ with certain phases ϕ, and $E_\xi^{(1)} = \mathrm{i}\lambda\langle\Psi_\xi|(\mathcal{PT})^{-1}(\mathcal{PT})V_p(\mathcal{PT})^{-1}(\mathcal{PT})|\Psi_\xi\rangle = -E_\xi^{(1)}$, provided that $|\Psi_\xi\rangle$ is not degenerate. This implies $E_\xi^{(1)} = 0$.

The second-order corrections of energy, $E_\xi^{(2)} = -\lambda^2\sum_{\tilde{\xi}\neq\xi}|\langle\Psi_\xi|V_p|\Psi_{\tilde{\xi}}\rangle|^2/(E_\xi - E_{\tilde{\xi}})$, thus become dominant. We assume that the energy gap between the two states $|\Psi_{\xi=e,g}\rangle$ becomes small (anticrossing) and even close when η is tuned. In the regime where the energy gap is small, we can assume that other levels are relatively far from $|\Psi_g\rangle$ and $|\Psi_e\rangle$. The above expression for $E_\xi^{(2)}$ implies that the dissipative perturbation leads to the higher eigenvalue E_e tending to decrease and the lower one E_g increasing. Then an energy gap tends to be closed by a dissipative perturbation, in contrast to the case of a Hermitian perturbation, which usually opens an energy gap or enhances the anticrossing effect.

Assuming the two levels whose energy gap is to be considered are $|\Psi_g\rangle$ and $|\Psi_e\rangle$ with $E_e > E_g$, when the perturbation strength $\lambda \ll \Delta E \equiv (E_e - E_g)$, the energy gap becomes small but is still real and finite. The spectra are still real, and the $\mathcal{PT}$ symmetry is unbroken. When $\Delta E \ll \lambda$, the dissipative perturbation becomes dominant, and degenerate perturbation can be approximately applicable. The perturbation matrix

$$M = i\lambda\begin{pmatrix}\langle\Psi_e|V_p|\Psi_e\rangle & \langle\Psi_e|V_p|\Psi_g\rangle \\ \langle\Psi_g|V_p|\Psi_e\rangle & \langle\Psi_g|V_p|\Psi_g\rangle\end{pmatrix} \tag{A3}$$

is a skew-Hermitian matrix satisfying $M^\dagger = -M$ and thus has purely imaginary spectra. The $\mathcal{PT}$ symmetry is broken in this regime.

Although the critical value of λ corresponding to the EPs that connect the broken and unbroken $\mathcal{PT}$ symmetry regimes cannot be fixed in the perturbation analysis, the form of $E_\xi^{(2)}$ indicates that it should occur when λ is comparable to the zero-order energy gap ΔE. Since λ is small, the breaking of $\mathcal{PT}$ symmetry will happen only in the small-gap regime of H_0. Therefore, a bubble breaking the $\mathcal{PT}$ symmetry, with imaginary spectra inside and two EPs at the ends, will emerge when the coupling strength η is tuned across the gap-closing points or anticross points with small minimum gap of H_0.

APPENDIX B: EXPERIMENTAL IMPLEMENTATION

The analogs of a generic $\mathcal{PT}$-symmetric model $H = \eta\sigma_z + \delta_0\sigma_0 + \delta_y\sigma_y + i\gamma\sigma_x$ with spin-dependent dissipations have been realized on different experimental platforms, including optical systems [46–48], ultracold atoms [49–51], ion traps [25,52], nitrogen-vacancy centers [34,53,54], and superconducting circuits [35,55–57]. For example, for superconducting circuits, such a model can be specifically realized with a dissipative qubit with a dissipation rate of κ_q. The dissipation process can be realized by coupling the qubit with a lossy resonator with a photonic decaying rate κ_r. When no photon

is leaked into the environment, the system's evolution is governed by the non-Hermitian Hamiltonian (setting $\hbar = 1$)

$$\mathcal{H}_{\rm NH} = \Omega(e^{i\theta}a^{\dagger}|g\rangle\langle e| + e^{-i\theta}a|e\rangle\langle g|) - \frac{i}{2}\kappa_r a^{\dagger}a - \frac{i}{2}\kappa_q|e\rangle\langle e|, \tag{B1}$$

where $|e\rangle$ ($|g\rangle$) denotes the upper (lower) level of the dissipative qubit, $a^{\dagger}$ (a) denotes the creation (annihilation) operator for the resonator modes, Ω denotes the coupling strength, and θ denotes the phase angle of the driving field. To modulate the coupling strength Ω and the phase angle θ in a preset sideband, an ac flux is applied to the qubit. The energy gap of the qubit is tuned as $\omega_q = \omega_0 + \varepsilon\cos(\nu t)$, where ω_0 is the mean $|e\rangle$-$|g\rangle$ energy difference and ε and ν denote the modulating amplitude and frequency, respectively. This property enables the system dynamics to be restricted within the reduced Hilbert subspace $\{|e, n-1\rangle, |g, n\rangle\}$ ($n \geqslant 1$) when the system initially has a definite quantum number, where the number in each ket denotes the photon number of the resonator. In such a subspace, we can redefine the basis vectors of the system as $|1\rangle = |e, n-1\rangle$, $|0\rangle = |g, n\rangle$. When we focus on the single-excitation case ($n = 1$), the Hamiltonian of the system can be rewritten as

$$\begin{aligned}\mathcal{H}_{\rm NH} &= \Omega(e^{i\theta}|0\rangle\langle 1| + e^{-i\theta}|1\rangle\langle 0|) - \frac{i}{2}\kappa_r|0\rangle\langle 0| - \frac{i}{2}\kappa_q|1\rangle\langle 1| \\ &= \Omega\cos(\theta)(|0\rangle\langle 1| + |1\rangle\langle 0|) \\ &\quad - \Omega\sin(\theta)(-i|0\rangle\langle 1| + i|1\rangle\langle 0|) \\ &\quad - \frac{i(\kappa_r + \kappa_q)}{4}(|0\rangle\langle 0| + |1\rangle\langle 1|) \\ &\quad - \frac{i(\kappa_r - \kappa_q)}{4}(|0\rangle\langle 0| - |1\rangle\langle 1|).\end{aligned} \tag{B2}$$

After rewriting it in the matrix form, we get

$$\begin{aligned}\mathcal{H}_{\rm NH} =& \Omega\cos(\theta)\sigma_x - \Omega\sin(\theta)\sigma_y - \frac{i(\kappa_r + \kappa_q)}{4}\sigma_0 \\ &- \frac{i(\kappa_r - \kappa_q)}{4}\sigma_z,\end{aligned} \tag{B3}$$

where $\sigma_x = |0\rangle\langle 1| + |1\rangle\langle 0|$, $\sigma_y = -i|0\rangle\langle 1| + i|1\rangle\langle 0|$, $\sigma_0 = |0\rangle\langle 0| + |1\rangle\langle 1|$, and $\sigma_z = |0\rangle\langle 0| - |1\rangle\langle 1|$. This is an analog of the generic $\mathcal{PT}$-symmetric Hamiltonian that we focus on in this work. If we adjust the coupling strength Ω and the phase angle θ, the corresponding nonadiabatic transitions should be observed in the experiment.

[1] C. M. Bender and S. Boettcher, Phys. Rev. Lett. **80**, 5243 (1998).

[2] R. El-Ganainy, K. G. Makris, M. Khajavikhan, Z. H. Musslimani, S. Rotter, and D. N. Christodoulides, Nat. Phys. **14**, 11 (2018).

[3] C. M. Bender, R. Tateo, P. E. Dorey, T. C. Dunning, G. Levai, S. Kuzhel, H. F. Jones, A. Fring, and D. W. Hook, *PT Symmetry in Quantum and Classical Physics* (World Scientific, Singapore, 2018).

[4] N. Moiseyev, *Non-Hermitian Quantum Mechanics* (Cambridge University Press, Cambridge, 2011).

[5] L. Feng, R. El-Ganainy, and L. Ge, Nat. Photonics **11**, 752 (2017).

[6] F. P. D. Pile, Nat. Photonics **11**, 742 (2017).

[7] M. F. Limonov, M. V. Rybin, A. N. Poddubny, and Y. S. Kivshar, Nat. Photonics **11**, 543 (2017).

[8] N. Horiuchi, Nat. Photonics **11**, 271 (2017).

[9] L. Xiao, K. Wang, X. Zhan, Z. Bian, K. Kawabata, M. Ueda, W. Yi, and P. Xue, Phys. Rev. Lett. **123**, 230401 (2019).

[10] F. Klauck, L. Teuber, M. Ornigotti, M. Heinrich, S. Scheel, and A. Szameit, Nat. Photonics **13**, 883 (2019).

[11] A. Szameit, M. C. Rechtsman, O. Bahat-Treidel, and M. Segev, Phys. Rev. A **84**, 021806(R) (2011).

[12] A. Regensburger, C. Bersch, M.-A. Miri, G. Onishchukov, D. N. Christodoulides, and U. Peschel, Nature (London) **488**, 167 (2012).

[13] B. Zhen, C. W. Hsu, Y. Igarashi, L. Lu, I. Kaminer, A. Pick, S.-L. Chua, J. D. Joannopoulos, and M. Soljačić, Nature (London) **525**, 354 (2015).

[14] S. Weimann, M. Kremer, Y. Plotnik, Y. Lumer, S. Nolte, K. G. Makris, M. Segev, M. C. Rechtsman, and A. Szameit, Nat. Mater. **16**, 433 (2017).

[15] K.-H. Kim, M.-S. Hwang, H.-R. Kim, J.-H. Choi, Y.-S. No, and H.-G. Park, Nat. Commun. **7**, 13893 (2016).

[16] A. Cerjan, A. Raman, and S. Fan, Phys. Rev. Lett. **116**, 203902 (2016).

[17] A. V. Poshakinskiy, A. N. Poddubny, and A. Fainstein, Phys. Rev. Lett. **117**, 224302 (2016).

[18] C. Dembowski, H.-D. Gräf, H. L. Harney, A. Heine, W. D. Heiss, H. Rehfeld, and A. Richter, Phys. Rev. Lett. **86**, 787 (2001).

[19] C. Dembowski, B. Dietz, H.-D. Gräf, H. L. Harney, A. Heine, W. D. Heiss, and A. Richter, Phys. Rev. E **69**, 056216 (2004).

[20] A. A. Mailybaev, O. N. Kirillov, and A. P. Seyranian, Phys. Rev. A **72**, 014104 (2005).

[21] J. Doppler, A. A. Mailybaev, J. Böhm, U. Kuhl, A. Girschik, F. Libisch, T. J. Milburn, P. Rabl, N. Moiseyev, and S. Rotter, Nature (London) **537**, 76 (2016).

[22] A. U. Hassan, G. L. Galmiche, G. Harari, P. LiKamWa, M. Khajavikhan, M. Segev, and D. N. Christodoulides, Phys. Rev. A **96**, 052129 (2017).

[23] A. U. Hassan, B. Zhen, M. Soljačić, M. Khajavikhan, and D. N. Christodoulides, Phys. Rev. Lett. **118**, 093002 (2017).

[24] X.-L. Zhang, S. Wang, B. Hou, and C. T. Chan, Phys. Rev. X **8**, 021066 (2018).

[25] Z. Ren, D. Liu, E. Zhao, C. He, K. K. Pak, J. Li, and G.-B. Jo, Nat. Phys. **18**, 385 (2022).

[26] J. Wiersig, Phys. Rev. A **93**, 033809 (2016).

[27] J. Wiersig, Phys. Rev. Lett. **112**, 203901 (2014).

[28] J. Wiersig, Photonics Res. **8**, 1457 (2020).

[29] H. Wang, L.-J. Lang, and Y. D. Chong, Phys. Rev. A **98**, 012119 (2018).

[30] B. Longstaff and E.-M. Graefe, Phys. Rev. A **100**, 052119 (2019).

[31] R. Okugawa and T. Yokoyama, Phys. Rev. B **99**, 041202(R) (2019).
[32] S. Sachdev, *Quantum Phase Transitions*, 2nd ed. (Cambridge University Press, Cambridge, 2011).
[33] J. Li, A. K. Harter, J. Liu, L. de Melo, Y. N. Joglekar, and L. Luo, Nat. Commun. **10**, 1 (2019).
[34] Y. Wu, W. Liu, J. Geng, X. Song, X. Ye, C.-K. Duan, X. Rong, and J. Du, Science **364**, 878 (2019).
[35] M. Naghiloo, M. Abbasi, Y. N. Joglekar, and K. Murch, Nat. Phys. **15**, 1232 (2019).
[36] J. C. Budich, J. Carlström, F. K. Kunst, and E. J. Bergholtz, Phys. Rev. B **99**, 041406(R) (2019).
[37] E. J. Bergholtz, J. C. Budich, and F. K. Kunst, Rev. Mod. Phys. **93**, 015005 (2021).
[38] M. Stålhammar and E. J. Bergholtz, Phys. Rev. B **104**, L201104 (2021).
[39] P. Delplace, T. Yoshida, and Y. Hatsugai, Phys. Rev. Lett. **127**, 186602 (2021).
[40] I. Mandal and E. J. Bergholtz, Phys. Rev. Lett. **127**, 186601 (2021).
[41] M. Abramowitz, I. A. Stegun, and R. H. Romer, *Handbook of Mathematical Functions with Formulas, Graphs, and Mathematical Tables* (American Association of Physics Teachers, College Park, 1988).
[42] X. Shen, F. Wang, Z. Li, and Z. Wu, Phys. Rev. A **100**, 062514 (2019).
[43] D. C. Brody, J. Phys. A **47**, 035305 (2014).
[44] K. D. Agarwal, T. K. Konar, L. G. C. Lakkaraju, and A. S. De, arXiv:2212.12403.
[45] M. M. Sternheim and J. F. Walker, Phys. Rev. C **6**, 114 (1972).
[46] H. Hodaei, A. U. Hassan, S. Wittek, H. Garcia-Gracia, R. El-Ganainy, D. N. Christodoulides, and M. Khajavikhan, Nature (London) **548**, 187 (2017).
[47] S. Yu *et al.*, Phys. Rev. Lett. **125**, 240506 (2020).
[48] K. Wang, L. Xiao, J. C. Budich, W. Yi, and P. Xue, Phys. Rev. Lett. **127**, 026404 (2021).
[49] Y.-L. Fang, J.-L. Zhao, Y. Zhang, D.-X. Chen, Q.-C. Wu, Y.-H. Zhou, C.-P. Yang, and F. Nori, Commun. Phys. **4**, 223 (2021).
[50] P. Peng, W. Cao, C. Shen, W. Qu, J. Wen, L. Jiang, and Y. Xiao, Nat. Phys. **12**, 1139 (2016).
[51] J. Li, A. K. Harter, J. Liu, L. de Melo, Y. N. Joglekar, and L. Luo, Nat. Commun. **10**, 855 (2019).
[52] W.-C. Wang *et al.*, Phys. Rev. A **103**, L020201 (2021).
[53] L. Ding, K. Shi, Q. Zhang, D. Shen, X. Zhang, and W. Zhang, Phys. Rev. Lett. **126**, 083604 (2021).
[54] W. Liu, Y. Wu, C.-K. Duan, X. Rong, and J. Du, Phys. Rev. Lett. **126**, 170506 (2021).
[55] W. Zhang, X. Ouyang, X. Huang, X. Wang, H. Zhang, Y. Yu, X. Chang, Y. Liu, D.-L. Deng, and L.-M. Duan, Phys. Rev. Lett. **127**, 090501 (2021).
[56] S. Dogra, A. A. Melnikov, and G. S. Paraoanu, Commun. Phys. **4**, 26 (2021).
[57] P.-R. Han *et al.*, Phys. Rev. Lett. **131**, 260201 (2023).